QCD thermodynamics with two flavors at $N_t = 6$

Claude Bernard and Michael C. Ogilvie
Department of Physics, Washington University, St. Louis, Missouri 63130

Thomas A. DeGrand
Department of Physics, University of Colorado, Boulder, Colorado 80309

Carleton DeTar
Department of Physics, University of Utah, Salt Lake City, Utah 84112

Steven Gottlieb and Alex Krasnitz
Department of Physics, Indiana University, Bloomington, Indiana 47405

R. L. Sugar
Department of Physics, University of California, Santa Barbara, California 93106-9530

D. Toussaint
Department of Physics, University of Arizona, Tucson, Arizona 85721
(Received 1 November 1991)

The first results of numerical simulations of quantum chromodynamics on the Intel iPSC/860 parallel processor are presented. We performed calculations with two flavors of Kogut-Susskind quarks at $N_t = 6$ with masses of $0.15T$ and $0.075T$ (0.025 and 0.0125 in lattice units) in order to locate the crossover from the low-temperature regime of ordinary hadronic matter to the high-temperature chirally symmetric regime. As with other recent two-flavor simulations, these calculations are insufficient to distinguish between a rapid crossover and a true phase transition. The phase transition is either absent or feeble at this quark mass. An improved estimate of the crossover temperature in physical units is given and results are presented for the hadronic screening lengths in both the high- and low-temperature regimes.

PACS number(s): 12.38.Gc, 11.15.Ha

I. INTRODUCTION

Numerical simulations currently hold the greatest theoretical promise for obtaining insight into the behavior of quantum chromodynamics at high temperature, starting from first principles. A crucial issue underlying phenomenological descriptions, and indeed predictions of experimental signatures, is whether or not a phase transition occurs between the low-temperature regime of ordinary hadronic matter and the high-temperature chirally symmetric regime. An important related issue is whether the mechanism of the phase transition or crossover is dominated by chiral-symmetry restoration or by deconfinement or both.

The occurrence of a phase transition depends on the number of quark flavors and their masses. When quark masses are heavy ($m_q \gg T$) they play only a small role in the statistical ensemble. It was suggested long ago, and recently confirmed with sophisticated techniques, that a first-order phase transition occurs in the pure glue ensemble [1]. Potts model simulations designed to imitate the QCD phase transition, however, showed that the occurrence of the deconfining phase transition depended sensitively on the presence of quarks in the thermal ensemble, weakening and disappearing as the quark mass was decreased [2]. At the limit of zero quark mass chiral-symmetry restoration becomes important. Renormalization-group arguments based on chiral models suggest that with three or more massless flavors a first-order chiral phase transition should occur [3]. For two massless quarks, however, the model prediction is less clear, and would allow merely a second-order transition.

Lattice simulations provide a means for resolving these questions, and considerable effort has been made to this end. There is clear evidence for a first-order transition for four flavors of light quarks; however, for two flavors of light quarks and for two light and one heavy quark there is no evidence for a first-order transition at quark masses and lattice spacings studied to date [4]. The data are consistent with a rapid crossover at finite quark mass, which might be associated with a second-order transition at $m_q = 0$. The question remains, whether this conclusion survives with increasing statistics, and, more importantly, with the approach to the continuum limit, which is reached by increasing N_t. Since these results were obtained with Kogut-Susskind fermions, for which the full flavor symmetry is recovered only in the continuum limit, one must also ask the related question of how badly flavor symmetry is violated.

In addition to determining the nature of the transition and the value of the crossover or critical temperature, simulations also help to characterize the different regimes. Through measurements of hadronic screening spectra, as well as the usual chiral order parameter, simulations have found that the high-temperature regime shows characteristics typical of chiral-symmetry restoration [5]. Such information is vital for the formulation of phenomenological models that extrapolate beyond the scope of numerical simulation and help in the experimental search for evidence of plasma formation.

The bulk of the simulations with two light flavors of Kogut-Susskind quarks have been carried out at $N_t=4$, which corresponds to a large lattice spacing. Preliminary studies have been made for $N_t=6$ [6] and 8 [7], and an extensive study is in progress for the latter case [8]. Extensive studies have also been made for two light and one heavy quark for $N_t=4$ and 6 [9]. In this paper we report on a simulation of high-temperature QCD with two light flavors of Kogut-Susskind quarks on $12^3\times 6$ lattices. Calculations were carried out with two quark masses $m_q=0.15T$ and $0.075T$ ($m_q=0.025a^{-1}$ and $0.0125a^{-1}$), where T is the temperature and a the lattice spacing. This calculation goes significantly beyond the work at $N_t=6$ reported in Ref. [6], and, when combined with a spectrum study at the same lattice spacing [10], provides a markedly improved estimated of the transition temperature at this lattice spacing.

The bulk of the simulations were carried out on the 32-node Intel iPSC/860 hypercube at the San Diego Supercomputer Center, which runs at a speed of approximately 16 Mflop per node with our present code. Some of the runs at $m_q=0.025a^{-1}$ were performed with our ST-100 array processor, giving us an opportunity to check the new iPSC/860 code. The iPSC/860 and the code are described briefly elsewhere [11]. We employ the hybrid-molecular-dynamics algorithm described in Ref. [12]. In integrating the molecular-dynamics equations of motion a time step of 0.02 is used for the heavier quark mass, and 0.01 for the lighter one. (We use the normalization of Ref. [12].) The momenta are refreshed and measurements taken at each 0.5 molecular dynamics time units. The limit on the conjugate-gradient residual was 0.001 25 per site for the heavier quark mass and 0.001 per site for the lighter one. The lengths of the runs are summarized in Tables I and II.

TABLE I. Data set for $m_q=0.025a^{-1}$. The second column shows the total number of molecular-dynamics time steps, and the third column the number for which screening mass measurements were made.

	Molecular-dynamics time units	
$6/g^2$	Total	With screening
5.40	1045	1045
5.425	1500	
5.44	1500	
5.45	1500	
5.46	1510	
5.48	1065	1065

TABLE II. Data set for $m_q=0.0125a^{-1}$. The second column shows the total number of molecular-dynamics time steps, and the third column the number for which screening mass measurements were made.

	Molecular-dynamics time units	
$6/g^2$	Total	With screening
5.40	1012	447
5.41	1002	847
5.42	1020	247
5.43	1025	370
5.44	1095	1095
5.45	930	930

II. RESULTS AND ANALYSIS

In Fig. 1 we show the time histories of the chiral order parameter $\langle\bar{\psi}\psi\rangle$ for the six values of $6/g^2$ which we ran at quark mass of $0.0125a^{-1}$. These time histories are typical of our result for both $m_q=0.025$ and 0.0125. No tunnelings are observed, but there is evidence for persistent fluctuations of large amplitude, suggesting near-critical behavior. Not surprisingly, calculations of the autocorrelation time for the physical observables also reflect this long-term trend. From autocorrelation functions for $\langle\bar{\psi}\psi\rangle$ and the real part of the Polyakov loop, we estimate the autocorrelation time to range from approximately 40 to 90 molecular-dynamics time units for the heavier quark mass, and 40–120 time units for the lighter one, the larger values occurring in the middle of the range of our $6/g^2$ values. Thus, at these $(6/g^2, am_q)$ values, it is important to make runs of at least the length of our data sample. Preequilibrium behavior is also evi-

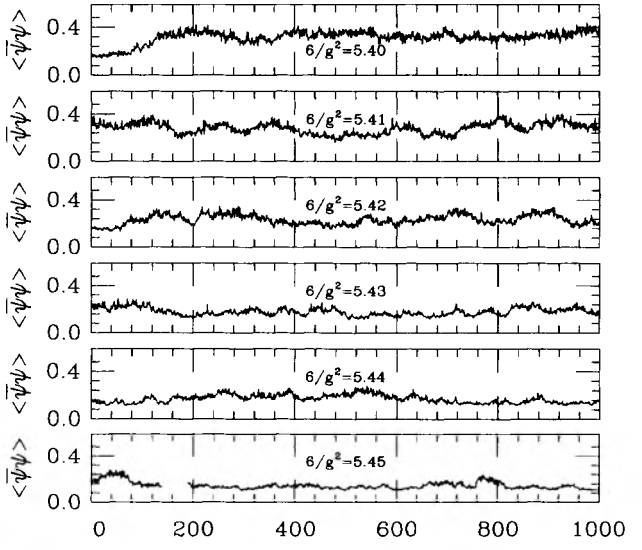

FIG. 1. The chiral order parameter $\langle\bar{\psi}\psi\rangle$ as a function of simulation time for $m_q=0.0125$ at six values of the gauge coupling. The small gap in the $6/g^2=5.45$ time history is due to the loss of a data file.

TABLE III. The chiral order parameter, the real part of the Polyakov loop, and the sum of the total energy and pressure for $m_q=0.025a^{-1}$.

$6/g^2$	$\bar{\psi}\psi$	ReP	$a^4(\epsilon+p)$
5.40	0.464(4)	0.027(3)	0.002(2)
5.425	0.375(8)	0.054(8)	0.005(1)
5.44	0.354(6)	0.067(7)	0.005(1)
5.45	0.268(7)	0.153(8)	0.012(1)
5.46	0.257(5)	0.163(8)	0.013(1)
5.48	0.229(7)	0.185(8)	0.017(3)

TABLE IV. The chiral order parameter, the real part of the Polyokov loop, and the sum of the total energy and pressure for $m_q=0.0125a^{-1}$.

$6/g^2$	$\bar{\psi}\psi$	ReP	$a^4(\epsilon+p)$
5.40	0.331(6)	0.045(4)	0.002(2)
5.41	0.275(15)	0.089(14)	0.009(2)
5.42	0.236(10)	0.107(12)	0.010(1)
5.43	0.175(10)	0.152(8)	0.014(2)
5.44	0.173(14)	0.150(13)	0.016(1)
5.45	0.136(7)	0.187(7)	0.018(1)

dent in the time histories. Accordingly, we remove data for the first 200 molecular-dynamics time units from each set prior to the computation of "equilibrium" averages.

Results for the average value of chiral order parameter $\langle\bar{\psi}\psi\rangle$, the Polyakov loop Re$P$, and for the sum of the energy and pressure are given in Tables III and IV. (The last quantity was chosen because unlike the energy and pressure individually, it does not require a zero-temperature subtraction.) Errors were obtained by binning the data in increasingly large bins, determining the standard deviation of the resulting binned sample, and extrapolating the result to infinite bin size.

A. Combining runs

The combined probability distribution for the energy and any other observable contains information about the expectation value of the observable at values of $6/g^2$ close to those used in the simulation. When simulations are available at several closely spaced values of the coupling constant, information from the different runs can be combined to produce an improved estimate of the observables, both at the values of $6/g^2$ where the simulations were run and at intermediate values [13]. Since we have runs at closely spaced values of $6/g^2$, we have used a method similar in spirit to Ref. [13] to combine and interpolate our runs.

The basic idea is to use the Monte Carlo data to construct an estimate of the partition function, and then to use this partition function to compute expectation values. Suppose we wish to study the expectation value of some operator P, such as the Polyakov loop. The partition function is

$$Z=\int[dU]\det(M[U])e^{-\beta E'[U]}\ . \tag{1}$$

Here β is $6/g^2$, not the inverse temperature $T^{-1}=aN_t$. $E'(U)$ is the extensive gauge field energy, or plaquette, with the sign convention that lower energies are favored. By introducing a δ function we can write the partition function in terms of a density of states.

$$Z=\int dE\,dP\int[dU]\delta(E-E'[U])\delta(P-P'[U])\det(M[U])e^{-\beta E'[U]}\ . \tag{2}$$

Since the density of states varies over many orders of magnitude, it is convenient to work with its logarithm $f(E,P)$:

$$Z=\int dE\,dP e^{f(E,P)}e^{-\beta E}\ , \tag{3}$$

where

$$e^{f(E,P)}=\int[dU]\delta(E-E'[U])\delta(P-P'[U])\det(M[U])\ . \tag{4}$$

Then

$$\langle P\rangle=\int dE\,dP P e^{-\beta E+f(E,P)}\ . \tag{5}$$

In the case of $\langle\bar{\psi}\psi\rangle$, where we use a noisy estimator constructed from a field of complex Gaussian random numbers, $\langle\bar{\psi}\psi\rangle_U=\langle R^\dagger M^{-1}R\rangle_{U,R}$, these formulas are modified only slightly:

$$\begin{aligned}Z&=\int[dR]e^{-R^\dagger R}\int[dU]\det(M[U])e^{-\beta E'[U]}\ ,\\&=\int dE\,dX\int[dR]e^{-R^\dagger R}\int[dU]\delta(E-E'[U])\delta(X-R^\dagger M^{-1}R)\det(M[U])e^{-\beta E'[U]}\ ,\\&=\int dE\,dX e^{f(E,X)}e^{-\beta E}\ ,\end{aligned} \tag{6}$$

where

$$e^{f(E,X)}=\int[dR]\int[dU]\delta(E-E'[U])\delta(X-R^\dagger M^{-1}R)e^{-R^\dagger R}\det(M[U])\ . \tag{7}$$

Now we must find the function $f(E,P)$ which best fits the Monte Carlo results. We choose to define "best fit" by a maximum-likelihood principle—we find $f(E,P)$, which maximizes the likelihood of getting the distribution our runs produced. It is in this choice of optimization criterion that our analysis differs from that of Ferrenberg and Swendsen [13]. If the samples were independent, this probability would be

$$\prod_r \prod_{i=1}^{N_r} \frac{\exp[-\beta_r E_{r,i}+f(E_{r,i},P_{r,i})]}{\int dE\,dP e^{-\beta_r E+f(E,P)}} . \tag{8}$$

Here r labels the runs, done with $\beta=\beta_r$, and i labels the samples in each run. Maximizing this probability is the same as minimizing its negative logarithm χ^2:

$$\chi^2=\sum_r \left| \sum_{i=1}^{N_r} [\beta_r E_{r,i}-f(E_{r,i},P_{r,i})] + N_r \ln \int dE\,dP\, e^{-\beta_r E+f(E,P)} \right| . \tag{9}$$

In minimizing χ^2 we weigh all our sample points equally. This is correct to the extent that the autocorrelation times are the same in all of the runs.

We must parametrize $f(E,P)$ using a reasonable number of parameters, which is small compared to the number of samples. We have experimented with two parametrizations for f, both based on specifying its value on a grid of points. To motivate the first parametrization, begin by dividing the range of E and P into bins, and setting f to a constant in each bin. The parameters are simply the values of f in the bins. The difficulty with the approach is that f is very strongly dependent on E. For the energies that are most important at a particular value of β, the exponent in Eq. (3) is at its peak, and $\partial f/\partial E \approx \beta$. Unless the energy bins are very small, approximating f by a constant would not be valid. In the six runs at $m_q=0.0125a^{-1}$ where β ranges from 5.40 to 5.45, the energy range on the $12^3\times 6$ lattice is about 1500, so with a reasonable number of bins for the energy, say 50, and β in the center of our range, 5.425, f should change by a factor of $e^{5.425\times 30}$ from one end of a bin to the other. Clearly a constant is a bad approximation. It would be equally easy to approximate f in each bin by a constant plus E times a bin-independent slope. Operationally this just corresponds to subtracting some constant $\bar{\beta}$ from β. With 50 bins for the energy this would still leave a discrepancy of $(1500/50)\times(\beta-\bar{\beta})/2 \approx 30\times 0.025/2 = 0.4$ across a bin, which means that the probability computed for a data point at the edge of a bin would be wrong by a factor of $e^{0.4}$. To deal with this problem, we adopt the approximation of moving all the E and P values to the center of the bin, and replacing the integral over the bin in the final term of Eq. (9) by the value in the center of the bin.

Now Eq. (9) simplifies somewhat:

$$\chi^2=\sum_r \left| -C(r,E,P)f(E,P)+N_r \ln \sum_{E,P} e^{-\beta_r E+f(E,P)} \right| , \tag{10}$$

where E and P now take a discrete set of values labeling the bins, $C(r,E,P)$ is the number of counts in bin E,P in run r, and we have dropped the term independent of f.

It is easy to check that this expression actually has a minimum. If any of the f become too small or too large χ^2 will start to increase. Also, it can be seen that adding a constant to all the f's, or multiplying the partition function by a constant, leaves χ^2 exactly unchanged. Finally, if the histograms from the different runs do not overlap a different constant can be added to the f's corresponding to each set of overlapping runs without changing χ^2.

A second approach that we have used is to make a bilinear interpolation of f on the E,P grid [14]. Here the parameters are the values of f at the points on the grid. At intermediate points f is defined by the bilinear interpolation formula [14]. This procedure has the advantage that there is no need to move the points to the center of the bins. However, in our particular application, we found that the results from the two approaches were indistinguishable, but the histogram method was somewhat simpler.

For this technique to be useful it is necessary that the histograms overlap (or that the relative weights of the nonoverlapping sectors be determined by other means). Figure 2 contains the energy histograms for the six runs at $m_q=0.0125a^{-1}$, showing that the energies overlap. In fact the two-dimensional (E,P) histograms also overlap.

Once f has been determined it is easy to calculate the expectation value of P at any value of β. In Fig. 3 we show the results for the Polyakov loop for the two values of the quark mass, and in Fig. 4 result for $\langle\bar{\psi}\psi\rangle$. The smooth curves are the results of fitting the density of states using the "histograms" ansatz. Again, nearly identical curves were obtained using bilinear extrapolation. Approximately 30 energy bins were used in these fits. The dotted lines above and below the curves are the error bars estimated from a jackknife procedure. In the jack-

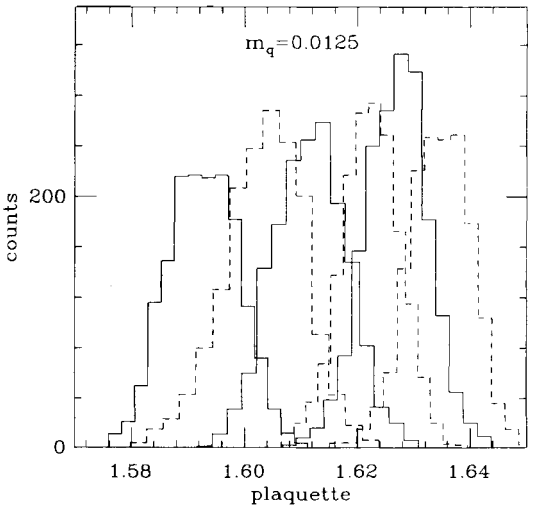

FIG. 2. Histograms of the energy (plaquette) for the six runs at $m_q=0.0125a^{-1}$. The values of $6/g^2$ for the histograms, going from left to right, are 5.40, 5.41, 5.42, 5.43, 5.44, and 5.45.

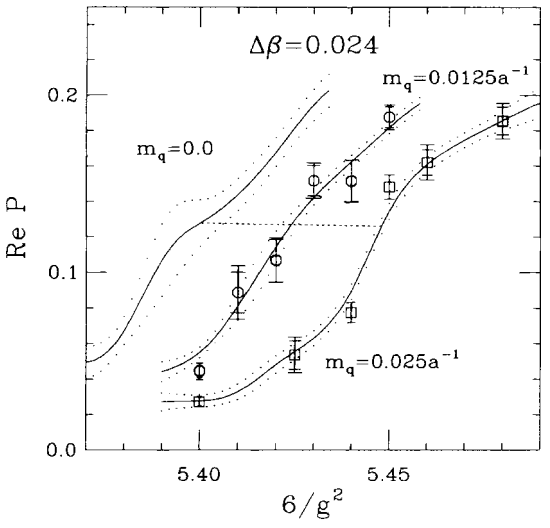

FIG. 3. The real part of the Polyakov loop. The symbols are the results from the individual runs, and the continuous curves labeled $m_q=0.025$ and 0.0125 are the results reconstructed from the estimate of the density of states. The curve labeled $m_q=0.0$ is an extrapolation from the two reconstructed curves. The dashed straight line shows a typical extrapolation.

knife we fit the data omitting the first fifth of each run, then omitting the second fifth, and so on, and estimated the error from the variance of the resulting pseudovalues. We repeated this procedure with ten divisions, and used the larger of the error estimates from the two calculations. The circles and squares are the values estimated from the individual runs. The smaller error bars on each symbol come from dividing the run into five blocks, so

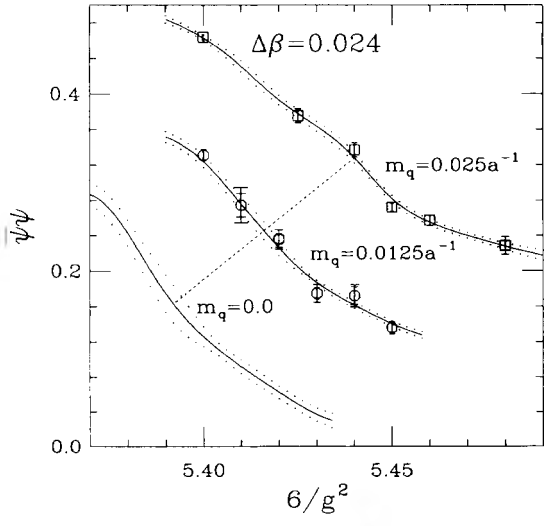

FIG. 4. The chiral order parameter $\langle\bar{\psi}\psi\rangle$. The symbols are the results of the individual runs, and the continuous curves labeled $m_q=0.025$ and 0.0125 are the results reconstructed from the estimate of the density of states. The curve labeled $m_q=0.0$ is an extrapolation from the two reconstructed curves. The dashed straight line shows a typical extrapolation.

they can be compared to the jackknife estimates of the error on the smooth curves. The larger error bars, which are quoted in Tables III and IV, come from an attempt to extrapolate the error estimates to an infinite block size. In most cases the two error estimates are virtually indistinguishable. The curves are certainly more indicative of a crossover than of a first-order phase transition.

In the absence of a phase transition, the crossover point $6/g_c^2$ is not well defined. We identify it as the point at which the slopes of the curves for the real part of the Polyakov loop and $\bar{\psi}\psi$ are largest. With this definition we estimate that $6/g_c^2$ lies between 5.44 and 5.45 for $m_q=0.025$ and between 5.41 and 5.43 for $m_q=0.0125$. As in all simulations with dynamical quarks performed to date, the quark masses with which we worked are unphysically large. Having obtained fits of the real part of the Polyakov loop and $\bar{\psi}\psi$ at two values of the quark mass, we can perform a linear extrapolation of these fits to smaller quark masses. It appears that the major effect of changing the quark mass between $m_q=0.025$ and 0.0125 is to shift the crossover coupling. Assuming that this would continue to be the case at smaller quark masses, we performed the extrapolation at a fixed value of $6/g^2-6/g_c^2$. Since the shift of $6/g_c^2$ between our two quark masses was approximately $\Delta\beta=0.024$, the extrapolation was performed using a value of $6/g^2$ that was 0.024 greater for the $m_q=0.025$ points than for the $m_q=0.0125$ points. The dotted straight lines in Figs. 3 and 4 show a typical extrapolation. The curves labeled $m_q=0$ in Figs. 3 and 4 were obtained from this extrapolation procedure. The errors bars shown for the $m_q=0$ curves indicate the uncertainty in the linear extrapolation parameters arising from the errors in the fits for $m_q=0.025$ and 0.0125. They do not include estimates of possible systematic errors arising from making a linear extrapolation over the range $0\le m_q\le 0.025$. Such an estimate would require, at a minimum, a calculation with a third value of the quark mass. Although highly desirable, that is beyond the scope of the present work. The $m_q=0$ curves must be considered qualitative in nature. They do not indicate a significant sharpening of the crossover as the quark mass is decreased.

B. Screening lengths

An important characteristic of the high-temperature phase at zero quark mass is the restoration of chiral symmetry. Symmetry restoration manifests itself in properties of the hadron propagators as well as in the degeneracy of the screening lengths of the chiral multiplets (π,σ), (ρ,a_1), and the nucleon and its parity partner (N,N') [5]. Thus, these quantities provide another signal for the crossover between the high- and low-temperature domains.

In a chiral-symmetric phase the fundamental excitations are expected to couple to operators with definite chiral properties such as $\bar{\psi}\Gamma(1+\gamma_5)\psi$, where Γ is a general Dirac matrix. On the other hand, in a chiral-broken phase, the fundamental excitations are expected to have definite parity, and therefore to couple equally to operators of opposite chirality. For example, in the scalar

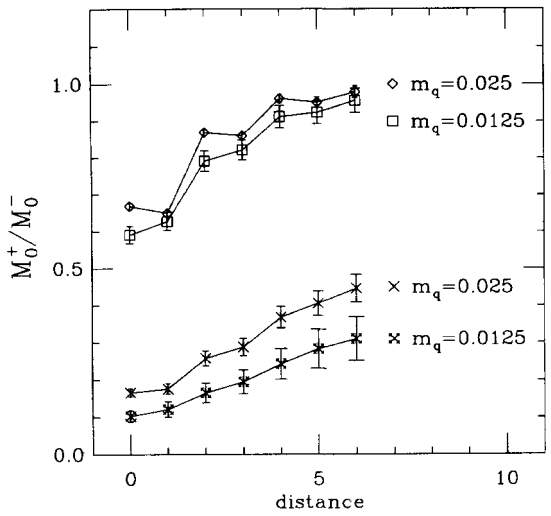

FIG. 5. The ratio of chiral projections for the spin-0 mesons. The diamonds and squares are for $6/g^2=5.40$ and $m_q=0.025$ and 0.0125, respectively. The crosses are for $6/g^2=5.48$ and $m_q=0.025$, and the fancy crosses for $6/g^2=5.45$ and $m_q=0.0125$.

and/or pseudoscalar channel,

$$M_0^{\pm}=\langle\bar{\psi}(x)(1\pm\gamma_5)\psi(x)\bar{\psi}(0)(1+\gamma_5)\psi(0)\rangle\ . \qquad (11)$$

In Fig. 5 we show M_0^+/M_0^- as a function of distance for the largest and smallest values of $6/g^2$ that we studied at each quark mass. The diamonds and squares are for $6/g^2=5.40$ and quark masses 0.025 and 0.0125, respectively. The approach of the ratio to one at a large distance is a clear signal that the lowest-mass excitation has definite parity and that chiral symmetry is broken. The plain crosses are the data for $6/g^2=5.48$ and $m_q=0.025$ while the fancy crosses are for $6/g^2=5.45$ and $m_q=0.0125$. Of course chiral symmetry is explicitly broken by the finite quark masses, but the decrease in M_0^+/M_0^- points to a restoration of chiral symmetry at zero quark mass.

The screening spectrum is found by measuring the hadron propagator in a spacelike direction [5]. We have made such measurements for all of the values of $6/g^2$ studied at $m_q=0.0125a^{-1}$, and at two values on either side of the crossover at $m_q=0.025a^{-1}$. The size of the data sample that included these measurements is listed in the last column of Tables I and II. (The limited data set for some values of $6/g^2$ is a result of the fact that the code for gauge fixing and measurement of the screening spectrum was completed only after the production runs had begun.) Spacelike hadron propagators at zero transverse momentum and minimum Matsubara frequency were measured from a wall source in a spacelike Coulomb gauge. The spectrum was determined through a global fit to the correlation data, taking into account correlations at different values of the separation from the source. The procedure for handling correlations is described in detail in Ref. [15]. Starting from data binned at 40 molecular-dynamics time units, an analysis of covariance was carried out. As a matter of principle, in view of the small data size, only the first three principal factors were kept. It was determined, however, that the results of the fits were not sensitive to this choice, giving variations consistent with the quoted errors as the number of retained principal factors was varied.

Results of the fits are given in Tables V–VII. The π and σ screening masses are plotted in Figs. 6. The errors quoted are statistical only. Statistical errors in the fitted masses were estimated from a combination of fits to large subsamples of the data and the error matrix of the fit. It is apparent from the $m_q=0.0125a^{-1}$ data that the (ρ,a_1)

TABLE V. Scalar-meson screening masses in lattice units as a function of $6/g^2$.

$6/g^2$	am_π	am_σ	$am_{\pi'}$
	$m_q=0.0125a^{-1}$		
5.40	0.337(8)	0.72(2)	0.62(3)
5.41	0.357(9)	0.680(12)	0.83(6)
5.42	0.39(2)	0.65(3)	0.76(6)
5.43	0.46(2)	0.58(1)	0.86(10)
5.44	0.455(14)	0.602(6)	0.87(6)
	$m_q=0.025a^{-1}$		
5.40	0.443(3)	1.02(2)	0.92(2)
5.48	0.605(8)	0.699(3)	1.11(8)

TABLE VI. Zero-helicity vector-meson screening masses in lattice units as a function of $6/g^2$.

$6/g^2$	am_ρ	am_{a_1}	$am_{\rho'}$	am_{b_1}
		$m_q=0.0125a^{-1}$		
5.40	1.29(15)	1.3(3)	0.97(6)	1.6(4)
5.41	1.02(6)	1.8(5)	1.15(5)	1.26(8)
5.42	1.3(2)	2.5(7)	1.26(10)	1.37(16)
5.43	0.97(4)	0.87(12)	1.04(3)	1.09(4)
5.44	1.19(6)	1.28(17)	1.04(2)	1.17(3)
5.45	1.10(6)	1.15(10)	1.05(2)	1.08(2)
		$m_q=0.025a^{-1}$		
5.40	1.10(4)	1.4(2)	1.14(3)	1.7(2)
5.48	1.04(3)	1.20(7)	1.07(1)	1.10(1)

TABLE VII. Nucleon screening masses in lattice units as a function of $6/g^2$.

$6/g^2$	am_N	$am_{N'}$
	$m_q=0.0125a^{-1}$	
5.40	1.45(6)	1.57(7)
5.41	1.56(4)	1.67(5)
5.42	1.50(9)	1.53(7)
5.43	1.54(3)	1.57(3)
5.44	1.54(2)	1.57(2)
5.45	1.58(1)	1.59(1)
	$m_q=0.025a^{-1}$	
5.40	1.62(2)	1.76(6)
5.48	1.586(7)	1.612(7)

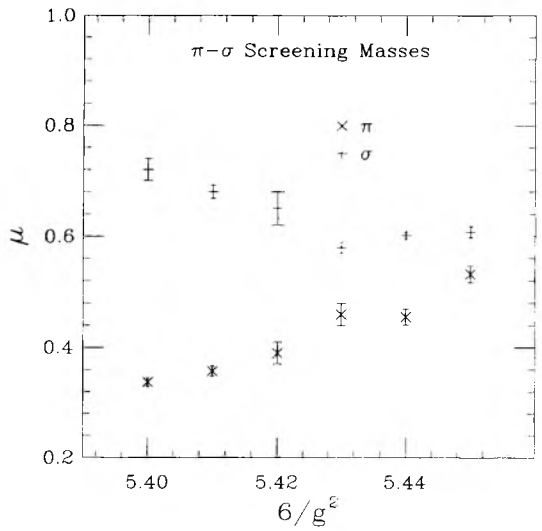

FIG. 6. The π and σ screening masses as a function of $6/g^2$ for $m_q=0.0125a^{-1}$.

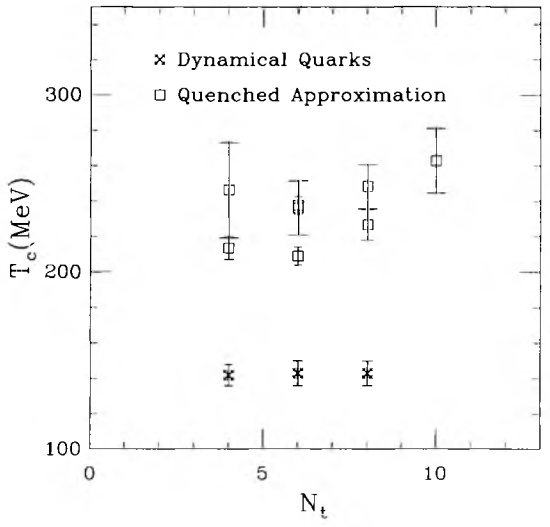

FIG. 7. The crossover temperature T_c in MeV as a function of N_t. The fancy crosses are for two flavors of dynamical quarks. The point at $N_t=4$ is from Ref. [6] and the one at $N_t=6$ from this work. The point at $N_t=8$ is from preliminary results of the $16^3\times 8$ study of Ref. [8] combined with an extrapolation of the spectrum results of Ref. [16]. The squares are quenched results using data from Refs. [17] and [18].

and (N,N') screening masses exhibit degeneracy for the most part for $6/g^2\geq 5.42$, although the errors are large for our data set. The screening masses for (π,σ), with considerably smaller errors, however, are separated over the entire range. However, rigorous degeneracy is expected only in the chiral limit of zero quark mass.

C. Transition temperature

By combining the above results with zero-temperature spectrum measurements at the same lattice spacing and quark mass, one can estimate the crossover temperature T_c from the relation [6]

$$T_c=\frac{m_E}{amN_t}\ . \tag{12}$$

The quantity m_E in the numerator of Eq. (12) is the mass of a hadron taken from experiment, am in the denominator is the mass of the same hadron in lattice units measured in the $T=0$ spectrum calculation at the same value of β, and N_t is the number of time slices in the thermodynamics calculation. We have carried out spectrum calculations at the crossover values of the gauge couplings for both $m_q=0.025$ and 0.0125 [10]. At the lighter quark mass these calculations have been performed on $12^3\times 24-$ lattices and at the heavier quark mass on lattices up to $16^3\times 24$. Here we use the ρ mass to set the energy scale. At $m_q=0.025$ we find $am_\rho=0.918\pm 0.005$, which gives $T_c=138\pm 1$, while at $m_q=0.0125$ we find $am_\rho=0.90\pm 0.02$ and $T_c=141\pm 3$. The error bars are a significant improvement over previously reported results at $N_t=6$. Of course these errors do not reflect any of the substantial systematics associated with lattice calculations at these values of the lattice spacing, where the ratio of proton to ρ mass obtained in simulations is 20% larger than the experimental value.

In Fig. 7 we plot T_c for two flavors of Kogut-Susskind quarks as a function of N_t using the ρ mass to set the energy scale. The results from simulations with dynamical quarks are denoted by fancy crosses, and those from the quenched approximation are denoted by squares. At present we have data for dynamical quarks only at $N_t=4$, 6, and 8. The point at $N_t=4$ is from Ref. [6], that at $N_t=6$ from the present work, and that at $N_t=8$ from preliminary results of a study on $16^3\times 8$ lattices [8] combined with spectrum calculation results of Ref. [16]. The quenched points were obtained by combining the quenched thermodynamics studies of Ref. [17] with quenched spectrum data of a number of groups [18]. In some cases more than one quenched result is shown, because more than one set of quenched spectrum calculations were available at the appropriate coupling. In making this figure we have extrapolated all thermodynamics and spectrum results to zero quark mass, except for the dynamical quark point at $N_t=8$. At this last point, we only have thermodynamics data at a quark mass of $m_q=0.0125$, so we have interpolated the spectrum results to this value. Even at $N_t=8$ we are not in the perturbative scaling regime. However, the insensitivity of T_c to N_t for both the quenched and dynamical calculations gives us some hope that these results are meaningful at least on a qualitative level. It is certainly clear that the full QCD values of T_c are significantly lower than those for the quenched approximation. It is important to push the measurement of T_c to the scaling regime since this quantity is of considerable physical importance, and is one of the few predictions of lattice gauge theory for which extensive experimental data do not already exist. It is also one of the few quantities calculated to date for which dynamical quarks appear to make a significant difference.

ACKNOWLEDGMENTS

Calculations were carried out on the Intel iPSC/860 hypercube at the San Diego Supercomputer Center. We wish to thank the SDSC staff, particularly Tom Metzger, Mike Wan, and Wayne Pfeiffer for their assistance. We also wish to thank personnel of Intel Scientific Computers, particularly Tony Anderson, Mike Barton, Roger Golliver, Victor Jackson, and Justin Rattner, for their assistance in the development of the code. This work was supported by the Department of Energy under Contracts No. DE-AC02-84ER-40125, No. DE-FC05-85ER-250000, and No. DE-FG02-85ER-40213, and by the National Science Foundation under Grants No. PHY86-14185, No. PHY90-08482, and No. PHY91-01853. Finally we express our appreciation for the hospitality extended to us by the Institute for Theoretical Physics, where part of this work was carried out.

[1] L. D. McLerran and B. Svetitsky, Phys. Lett. **98B**, 105 (1981); A. D. Kennedy, J. Kuti, S. Meyer, and B. J. Pendleton, Phys. Rev. Lett. **54**, 87 (1985); S. A. Gottlieb, J. Kuti, D. Toussaint, A. D. Kennedy, S. Meyer, B. J. Pendleton, and R. L. Sugar, *ibid.* **55**, 1958 (1985); N. H. Christ and A. E. Terrano, *ibid.* **58**, 111 (1985); A. Ukawa, in *Lattice '89,* Proceedings of the International Symposium, Capri, Italy, 1989, edited by R. Petronzio *et al.* [Nucl. Phys. B (Proc. Suppl.) **17**, 118 (1990)]; and references contained therein.

[2] T. DeGrand and C. DeTar, Nucl. Phys. **B225** [FS9], 590 (1983).

[3] R. D. Pisarski and F. Wilczek, Phys. Rev. D **29**, 338 (1984).

[4] For a recent review of the present status of finite-temperature QCD simulations, see S. Gottlieb, in *Lattice '90,* Proceedings of the International Symposium, Tallahassee, Florida, 1990, edited by U. M. Heller, A. D. Kennedy, and S. Sanielevici [Nucl. Phys. B (Proc. Suppl.) **20**, 247 (1991)].

[5] C. DeTar and J. B. Kogut, Phys. Rev. Lett. **59**, 399 (1987); Phys. Rev. D **36**, 2828 (1987); S. Gottlieb, W. Liu, D. Toussaint, R. L. Renken, and R. L. Sugar, Phys. Rev. Lett. **59**, 1881 (1987). A. Gocksch, P. Rossi, and U. Heller, Phys. Lett. B **205**, 334 (1988).

[6] S. Gottlieb, W. Liu, D. Toussaint, R. L. Renken, and R. L. Sugar, Phys. Rev. Lett. **59**, 1513 (1987).

[7] S. Gottlieb, W. Liu, D. Toussaint, R. L. Renken, and R. L. Sugar, Phys. Rev. D **41**, 622 (1990).

[8] S. Gottlieb, U. M. Heller, A. D. Kennedy, J. B. Kogut, A. Krasnitz, W. Liu, R. L. Renken, D. K. Sinclair, R. L. Sugar, D. Toussaint, and K. C. Wang (unpublished).

[9] F. R. Brown *et al.,* Phys. Rev. Lett. **65**, 2491 (1990); J. B. Kogut, D. K. Sinclair, and K. C. Wang, Phys. Lett. B **263**, 101 (1991).

[10] C. Bernard, T. A. DeGrand, C. DeTar, S. Gottlieb, A. Krasnitz, M. C. Ogilvie, R. L. Sugar, and D. Toussaint (unpublished).

[11] C. Bernard, T. DeGrand, C. DeTar, S. Gottlieb, A. Krasnitz, M. C. Ogilvie, R. L. Sugar, and D. Toussaint, in *Workshop on Fermion Algorithms,* edited by H. J. Hermann and F. Karsch (World Scientific, Singapore, 1991).

[12] S. Gottlieb, W. Liu, D. Toussaint, R. L. Renken, and R. L. Sugar, Phys. Rev. D **35**, 2531 (1987).

[13] A. M. Ferrenberg and R. H. Swendsen, Phys. Rev. Lett. **63**, 1195 (1989).

[14] W. Press, B. Flannery, S. Teukolsky, and W. Vetterling, *Numerical Recipes* (Cambridge University Press, Cambridge, England, 1986).

[15] T. A. DeGrand and C. E. DeTar, Phys. Rev. D **34**, 2469 (1986); DeTar and Kogut [5]; S. Gottlieb, W. Liu, R. L. Renken, R. L. Sugar, and D. Toussaint, Phys. Rev. D **38**, 2245 (1988).

[16] HEMCGC Collaboration, K. M. Bitar *et al.,* Phys. Rev. Lett. **65**, 2106 (1990); Phys. Rev. D **42**, 3794 (1990); F. R. Brown *et al.,* Phys. Rev. Lett. **67**, 1062 (1991).

[17] A. D. Kennedy, J. Kuti, S. Meyer, and B. J. Pendleton, Phys. Rev. Lett. **54**, 87 (1985); S. A. Gottlieb, J. Kuti, D. Toussaint, A. D. Kennedy, S. Meter, B. J. Pendleton, and R. L. Sugar, *ibid.* **55**, 1958 (1985).

[18] P. Bacilieri *et al.,* Nucl. Phys. **B343**, 228 (1990); S. Cabasino *et al.,* in *Lattice '90* [4], p. 399; R. Gupta *et al.,* Phys. Rev. D **43**, 2003 (1991); K. M. Bitar *et al.,* in *Lattice '90* [4], p. 362.